Taylor & Francis
Taylor & Francis Group

A multi-objective topology optimisation for 2D electro-magnetic wave problems with the level set method and BEM

Hiroshi Isakari [ID], Kenta Nakamoto [ID], Tatsuya Kitabayashi [ID], Toru Takahashi and Toshiro Matsumoto

Department of Mechanical Engineering, Nagoya University, Aichi, Japan

ABSTRACT

We have been investigating applications of a level set-based topology optimisation for wave devices with the boundary element method. For two-dimensional electro-magnetic wave problems, we have, so far, proposed a topology optimisation which can find a configuration of dielectric materials to locally minimise an objective functional such as the intensity of transverse electric (TE) or transverse magnetic (TM) polarised wave with a specific frequency. As an extension of our methodology, this paper presents a multi-objective topology optimisation, which can deal with some objective functionals simultaneously. The present method, for instance, can find a material distribution which can locally minimise the intensity of both TM and TE waves with multiple frequencies. The basic idea of the proposed method is to use the weighted sum or the Kreisselmeier–Steinhause function of the original objective functionals as a new objective functional. We present a derivation of the topological derivative for the new objective functional, and a detailed algorithm of the optimisation process with the derived topological derivative. We also present some numerical examples to illustrate the validity and efficiency of the proposed method.

1. Introduction

Structural optimisations have intensively been studied, and have successfully been applied to design problems in some engineering fields. The topology optimisation (Bendsøe & Kikuchi, 1988) is now considered to be the most flexible optimal design method among structural optimisations since it can design not only the shape but also the topology (i.e. the number of holes or inclusions) of devices. Since the original aim of the topology optimisation was to design stiff materials with a preset volume constrain, the topology optimisation has been developed mainly in the field of structural mechanics (Bendsøe & Kikuchi,

1988; Sethian & Wiegmann, 2000; Wang, Wang, & Guo, 2003; Yamada, Izui, Nishiwaki, & Takezawa, 2010).

Recently, one of the main trends in the community of the optimal design is to enhanced the applicability of the topology optimisation to problems in various engineering fields other than structural mechanics, such as thermal problems (Jing, Isakari, Matsumoto, Yamada, & Takahashi, 2015; Yamada, Izui, & Nishiwaki, 2011), fluid problems (Papoutsis-Kiachagias & Giannakoglou, 2015; Yaji et al., 2014), wave problems (Isakari et al., 2014; Jensen, 2007; Novotny, Feijóo, Taroco, & Padra, 2007), etc. Let us review some publications for topology optimisations in wave problems. Jensen (2007) proposed a topology optimisation to manipulate reflection and dissipation of elastic waves, and Byun and Park (2007) designed a waveguide for electromagnetic waves, both of which employ a continuous material function as the design variable. When the continuous material function is used, the obtained material distribution may suffer from so-called grayscale problems. In order to overcome the grayscale problem, Otomori et al. (2013) utilised the level set function (Wang et al., 2003; Yamada et al., 2010) to design optical cloaks. With the level set function, they have successfully designed optimal cloaks with clear boundaries. We think, however, that the applicability of the above methods to real engineering problems is still limited because all of them utilise the finite element method (FEM) to solve the wave problems involved in the process of the sensitivity analysis. When the FEM is utilised to solve wave scattering problems in an unbounded domain, the unbounded domain is approximated with a large one, which leads to unexpected large-scale problems. Further, an artificial boundary condition, such as perfect matched layer (PML) (Turkel & Yefet, 1998), is required to let the numerical solutions satisfy the radiation condition. Thus, the domain-type solvers like FEM are not suitable for optimisation problems in wave problems.

To overcome the difficulties to deal with the wave problem in unbounded domain, we have been investigating applications of a level set-based topology optimisation for wave devices with the boundary element method (BEM). When the BEM is utilised for wave problems, the unbounded domain can exactly be expressed with the small number of elements since only boundary element mesh is required in the BEM, and the numerical solution automatically satisfies the radiation condition. We have developed topology optimisations for sound waves in 3D (Isakari et al., 2014; Kondo, Isakari, Takahashi, & Matsumoto, 2014) and electro-magnetic wave problems in 2D (Abe, Isakari, Takahashi, & Matsumoto, 2013) and in 3D (Kourogi, Isakari, Takahashi, Yamada, & Matsumoto, 2013). We have, so far, got stuck in so-called single-objective optimisation problems, in which a single-objective functional is considered. In Abe et al. (2013), the objective functional is defined as the intensity of either transverse electric (TE) or transverse magnetic (TM) polarised wave with a specific frequency at some observation points. In order to use the topology optimisation to design industrial products, it is important, for instance, to minimise the intensity of both TM and
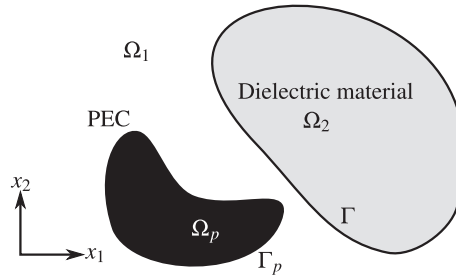
Figure 1. Domains.

TE waves with multiple frequencies. We propose, in this paper, a multi-objective optimisation method to find a configuration of dielectric material(s) which minimises multiple objective functionals in two-dimensional electro-magnetic wave problems.

The paper is organised as follows. After reviewing the fundamental equations for two-dimensional electro-magnetic wave problems in Section 2.1, the topological derivative, which characterises the sensitivity of objective functionals to a change of the topology, for multiple objective functionals is presented in Section 2.2. Section 2.3 is devoted to present the fast multipole boundary element method (FMBEM) which is utilised to evaluate the topological derivative. In Section 3, we present the formulation of the proposed topology optimisation method by the topological derivative along with a detailed re-meshing procedure in the optimisation problems. We show some numerical examples to show the validity and the efficiency of the proposed methodology in Section 4, and summarise the paper in Section 5.

2. Topological derivative and its numerical evaluation

In this section, we derive the topological derivative (Novotny, Feijóo, Taroco, & Padra, 2003) for multi-objective optimisation problems, and present a numerical method to evaluate the topological derivative with the FMBEM.

2.1. Electro-magnetic wave problems in $\mathbb{R}^2$

In this subsection, we review fundamental equations for electro-magnetic wave problems in $\mathbb{R}^2$.

Let us consider a domain defined in Figure 1. Ω_i ($i = 1, 2$) is filled with a dielectric material with permittivity ε_i and permeability μ_i while Ω_p is filled with perfect electrical conductor (PEC), both of which are uniform in x_3 direction. We assume that Ω_1 is an infinite domain, and Ω_2 and Ω_p are bounded. We denote $\partial\Omega$ and $\partial\Omega_p$ as Γ and Γ_p, respectively.

When $\Omega := \overline{\Omega_1 \cup \Omega_2 \cup \Omega_p}$ is impinged by the TE incident wave $H^{\mathrm{in}} = (0, 0, u^{\mathrm{in}})^t$, the total magnetic field $H = (0, 0, u)^t$ is governed by the following equations:

$$\nabla^2 u(x) + k_i^2 u(x) = 0 \quad x \in \Omega_i \ (i = 1, 2), \tag{1}$$

$$\lim_{x \in \Omega_1 \to x \in \Gamma} u(x) = \lim_{x \in \Omega_2 \to x \in \Gamma} u(x), \tag{2}$$

$$\lim_{x \in \Omega_1 \to x \in \Gamma} \left(\frac{1}{\varepsilon_1} \frac{\partial u(x)}{\partial n} \right) = \lim_{x \in \Omega_2 \to x \in \Gamma} \left(\frac{1}{\varepsilon_2} \frac{\partial u(x)}{\partial n} \right), \tag{3}$$

$$\frac{\partial u(x)}{\partial n} = 0 \quad x \in \Gamma_p, \tag{4}$$

$$u(x) \to u^{\mathrm{in}}(x) \quad \text{as} \quad |x| \to \infty, \tag{5}$$

where $k_i := \omega \sqrt{\varepsilon_i \mu_i}$ is the wave number, ω is the angular frequency and n is the outward normal vector of Ω on $\overline{\Gamma \cup \Gamma_p}$. When Ω is impinged by the TM incident wave $E^{\mathrm{in}} = (0, 0, v^{\mathrm{in}})^t$, the total electric field $E = (0, 0, v)^t$ is governed by the following equations:

$$\nabla^2 v(x) + k_i^2 v(x) = 0 \quad x \in \Omega_i \ (i = 1, 2), \tag{6}$$

$$\lim_{x \in \Omega_1 \to x \in \Gamma} v(x) = \lim_{x \in \Omega_2 \to x \in \Gamma} v(x), \tag{7}$$

$$\lim_{x \in \Omega_1 \to x \in \Gamma} \left(\frac{1}{\mu_1} \frac{\partial v(x)}{\partial n} \right) = \lim_{x \in \Omega_2 \to x \in \Gamma} \left(\frac{1}{\mu_2} \frac{\partial v(x)}{\partial n} \right), \tag{8}$$

$$v(x) = 0 \quad x \in \Gamma_p, \tag{9}$$

$$v(x) \to v^{\mathrm{in}}(x) \quad \text{as } |x| \to \infty. \tag{10}$$

We henceforth denote the boundary value problems (1)–(5) and (6)–(10) as TE problem and TM problem, respectively. Note that functions u and v are considered to be independent solutions of two-dimensional electro-magnetic wave problems.

The TM and TE problems can be written in the following unified notation:

$$\alpha_i \nabla^2 w(x) + \beta_i w(x) = 0 \quad x \in \Omega_i \ (i = 1, 2), \tag{11}$$

$$\lim_{x \in \Omega_1 \to x \in \Gamma} w(x) = \lim_{x \in \Omega_2 \to x \in \Gamma} w(x), \tag{12}$$

$$\lim_{x \in \Omega_1 \to x \in \Gamma} \left(\alpha_1 \frac{\partial w(x)}{\partial n} \right) = \lim_{x \in \Omega_2 \to x \in \Gamma} \left(\alpha_2 \frac{\partial w(x)}{\partial n} \right), \tag{13}$$

$$(\gamma w)(x) = 0 \quad x \in \Gamma_p, \tag{14}$$

$$w(x) \to w^{\mathrm{in}}(x) \quad \text{as } |x| \to \infty, \tag{15}$$

where w, α_i, β_i ($i = 1, 2$) and γ are chosen, in the case of TE problem, as

$$w = u \tag{16}$$

$$\alpha_i = \frac{1}{\varepsilon_i}, \tag{17}$$

$$\beta_i = \omega^2 \mu_i, \tag{18}$$

$$\gamma = \frac{\partial}{\partial n}, \tag{19}$$

and, in the case of TM problem, as:

$$w = v \tag{20}$$

$$\alpha_i = \frac{1}{\mu_i}, \tag{21}$$

$$\beta_i = \omega^2 \varepsilon_i, \tag{22}$$

$$\gamma = 1. \tag{23}$$

2.2. Topological derivative of multi-objective functionals

In this section, let us present the topological derivative of an objective functional for multi-objective optimisation problems. We consider, for example, the following composite function $\mathcal{J}$ of two objective functionals J_e and J_m:

$$\mathcal{J} = \mathcal{F}(J_e, J_m), \tag{24}$$

where $\mathcal{F}$ is a functional, and J_e and J_m have the following representations:

$$J_e = \frac{1}{2} \sum_{m=1}^{M} f(u(x_m^{\mathrm{obs}})), \tag{25}$$

$$J_m = \frac{1}{2} \sum_{m=1}^{M} f(v(x_m^{\mathrm{obs}})), \tag{26}$$

where u and v are solutions of TE problem (1)–(5) and TM problem (6)–(10), respectively. Also, f is a functional, and x_m^{obs} ($m = 1, \ldots, M$) is an observation point where the functional f is defined.

The rest of this subsection is devoted to derive the topological derivative of the objective functional (24). To this end, we first evaluate the topological derivative of the following functional J:

$$J = \frac{1}{2} \sum_{m=1}^{M} f(w(x_m^{\mathrm{obs}})), \tag{27}$$

where w, which represents either magnetic or electric field, is a solution of the boundary value problem (11)–(15).

The topological derivative $\mathcal{T}$ is defined as follows:

$$\delta J(x) = \mathcal{T}(x)a(r) + o(a(r)) \quad x \in \overline{\Omega_1 \cup \Omega_2}, \tag{28}$$

where $\delta J(x)$ represents a perturbation of the objective functional J when an infinitesimal circular dielectric material of radius r with material constants of (ε_1, μ_1) is introduced in $x \in \Omega_2$ (or, an infinitesimal circular dielectric material with (ε_2, μ_2) is introduced in $x \in \Omega_1$), and $a(r)$ is a monotonically increasing function for $r > 0$. Let us now evaluate the perturbation δJ, which is associated with the perturbation δw of w as follows (Isakari et al., 2014):

$$\delta J = \Re \left[\sum_{m=1}^{M} \frac{\partial f(x_m^{\text{obs}})}{\partial w} \delta w(x_m^{\text{obs}}) \right]. \tag{29}$$

In the case that Ω_r with (ε_2, μ_2) appears on $x \in \Omega_1$, and w becomes as $w(x) + \delta w(x)$ for $x \in \Omega_i$ $(i = 1, 2)$ and $\hat{w}(x)$ for $x \in \Omega_r$, δw and $\hat{w}$ are governed by the following boundary value problem:

$$\alpha_1 \nabla^2 \delta w(x) + \beta_1 \delta w(x) = 0 \quad x \in \Omega_1 \setminus \overline{\Omega_r}, \tag{30}$$

$$\alpha_2 \nabla^2 \delta w(x) + \beta_2 \delta w(x) = 0 \quad x \in \Omega_2, \tag{31}$$

$$\alpha_2 \nabla^2 \hat{w}(x) + \beta_2 \hat{w}(x) = 0 \quad x \in \Omega_r, \tag{32}$$

$$\lim_{x \in \Omega_1 \to x \in \Gamma} \delta w(x) = \lim_{x \in \Omega_2 \to x \in \Gamma} \delta w(x), \tag{33}$$

$$\lim_{x \in \Omega_1 \to x \in \Gamma_r} (w(x) + \delta w(x)) = \lim_{x \in \Omega_2 \to x \in \Gamma_r} \hat{w}(x), \tag{34}$$

$$\lim_{x \in \Omega_1 \to x \in \Gamma} \left(\alpha_1 \frac{\partial \delta w(x)}{\partial n} \right) = \lim_{x \in \Omega_2 \to x \in \Gamma} \left(\alpha_2 \frac{\partial \delta w(x)}{\partial n} \right), \tag{35}$$

$$\lim_{x \in \Omega_1 \to x \in \Gamma_r} \left(\alpha_1 \frac{\partial (w(x) + \delta w(x))}{\partial n} \right) = \lim_{x \in \Omega_2 \to x \in \Gamma_r} \left(\alpha_2 \frac{\partial \hat{w}(x)}{\partial n} \right), \tag{36}$$

$$(\gamma(w + \delta w))(x) = 0 \quad x \in \Gamma_p, \tag{37}$$

$$\delta w(x) \to 0 \quad \text{as } |x| \to \infty, \tag{38}$$

where Γ_r represents $\partial \Omega_r$. Note that, if we use (29) to evaluate δJ, δw is required to be evaluated on all observation points x_m^{obs}, $(m = 1, \ldots, M)$, which is totally impractical. That requires to solve the boundary value problem (30)–(38) as is. In order to eliminate $\delta w(x_m^{\text{obs}})$ in the expression for δJ in Equation (29), an adjoint variable $\tilde{w}$, which is governed by the following boundary value problem (Bonnet & Nemitz, 2007), is introduced:

$$\alpha_i \nabla^2 \tilde{w}(x) + \beta_i \tilde{w}(x) + \delta_{1i} \sum_{m=1}^{M} \frac{\partial f(x_m^{\mathrm{obs}})}{\partial w} \delta(x - x_m^{\mathrm{obs}}) = 0 \quad x \in \Omega_i, \tag{39}$$

$$\lim_{x \in \Omega_1 \to x \in \Gamma} \tilde{w}(x) = \lim_{x \in \Omega_2 \to x \in \Gamma} \tilde{w}(x), \tag{40}$$

$$\lim_{x \in \Omega_1 \to x \in \Gamma} \left(\alpha_1 \frac{\partial \tilde{w}(x)}{\partial n} \right) = \lim_{x \in \Omega_2 \to x \in \Gamma} \left(\alpha_2 \frac{\partial \tilde{w}(x)}{\partial n} \right), \tag{41}$$

$$(\gamma \tilde{w})(x) = 0 \quad x \in \Gamma_p, \tag{42}$$

$$\tilde{w}(x) \to 0 \quad \text{as } |x| \to \infty, \tag{43}$$

where $\delta(x)$ is the Dirac delta. Note that, to derive the adjoint Equation (39), we have assumed $x_m^{\mathrm{obs}} \in \Omega_1$. $\delta w(x_m^{\mathrm{obs}})$ in Equation (29) can be replaced by the adjoint variable $\tilde{w}$ with the help of the reciprocal theorem. In the limit of $r \to 0$, δJ is asymptotically expressed (Carpio & Rapún, 2008) as follows:

$$\delta J(x) = \Re \left[\frac{2\alpha_1(\alpha_1 - \alpha_2)}{\alpha_1 + \alpha_2} \sum_{j=1}^{2} \frac{\partial w(x)}{\partial x_j} \frac{\partial \tilde{w}(x)}{\partial x_j} + (\beta_2 - \beta_1) w(x) \tilde{w}(x) \right]$$
$$\times \int_{\Omega_r} d\Omega + o(r^2). \tag{44}$$

By comparing Equation (28) with Equation (44), we have the topological derivative of the single-objective functional in Equation (27) as follows:

$$\mathcal{T}(x) = \Re \left[\frac{2\alpha_1(\alpha_1 - \alpha_2)}{\alpha_1 + \alpha_2} \sum_{j=1}^{2} \frac{\partial w(x)}{\partial x_j} \frac{\partial \tilde{w}(x)}{\partial x_j} + (\beta_2 - \beta_1) w(x) \tilde{w}(x) \right]. \tag{45}$$

Note that we have chosen $a(r)$ in Equation (28) as $a(r) = \pi r^2$.

In this study, we employ $\mu_i = 1$ $(i = 1, 2)$ as is often the case. Then, the topological derivative $\mathcal{T}_e$ of the objective functional J_e in Equation (25) for the TE problem is represented as:

$$\mathcal{T}_e(x) = \Re \left[\frac{2(\varepsilon_2 - \varepsilon_1)}{\varepsilon_1(\varepsilon_2 + \varepsilon_1)} \sum_{j=1}^{2} \frac{\partial \tilde{u}(x)}{\partial x_j} \frac{\partial u(x)}{\partial x_j} \right], \tag{46}$$

and the topological derivative $\mathcal{T}_m$ in TM problem is represented as:

$$\mathcal{T}_m(x) = \Re[\omega^2 (\varepsilon_2 - \varepsilon_1) \tilde{v}(x) v(x)], \tag{47}$$

where $\tilde{u}$ and $\tilde{v}$ are the solutions of the adjoint problem (39)–(43) with Equations (17)–(19) and Equations (21)–(23), respectively. In the case that an infinitesimal

material with (ε_1, μ_1) appears in Ω_2, the associated topological derivative can be obtained by interchanging (ε_1, μ_1) and (ε_2, μ_2) in the expressions (46) and (47).

The topological derivative $\mathcal{T}$ of the composite function (24) can be evaluated with the following chain rule:

$$\mathcal{T} = \frac{\partial \mathcal{F}}{\partial J_e} \mathcal{T}_e + \frac{\partial \mathcal{F}}{\partial J_m} \mathcal{T}_m, \tag{48}$$

where the partial derivatives can be evaluated in a standard manner.

In multi-objective optimisations, the weighted sum of objective functionals $\mathcal{J}_{sum}$ with some constants c_e and c_m as:

$$\mathcal{J}_{sum} = c_e J_e + c_m J_m, \tag{49}$$

is often used as the objective functional. According to Equation (48), the topological derivative $\mathcal{T}_{sum}$ of the weighted sum (49) is evaluated as follows:

$$\mathcal{T}_{sum} = c_e \mathcal{T}_e + c_m \mathcal{T}_m. \tag{50}$$

Another possible choice of the multi-objective functional can be, for example, the Kreisselmeier–Steinhause (KS) function which enables us to minimise $\max\{J_e, J_m\}$, represented as follows:

$$\mathcal{J}_{KS} = \ln \left(\exp \left(c_e J_e \right) + \exp \left(c_m J_m \right) \right), \tag{51}$$

and the topological derivative for (51) is evaluated by Equation (48) as follows:

$$\mathcal{T} = \frac{c_e \mathcal{T}_e \exp \left(c_e J_e \right) + c_m \mathcal{T}_m \exp \left(c_m J_m \right)}{\exp \left(w_e J_e \right) + \exp \left(w_m J_m \right)}. \tag{52}$$

Above formulations for the topological derivative (48) can trivially be extended to a more general objective function $\mathcal{J} = \mathcal{F}(J_1, J_2, \ldots, J_n)$ of the arbitrary number n of objective functions J_i $(i = 1, \ldots, n)$ as $\mathcal{T} = \sum_{i=1}^{n} \frac{\partial \mathcal{F}}{\partial J_i} \mathcal{T}_i$, where $\mathcal{T}_i$ represents the topological derivative of J_i.

2.3. The fast multipole boundary element method

In order to evaluate the topological derivatives (50) or (52), it is required to solve the forward (11)–(13) and the adjoint (39)–(41) problems, both of which are defined in an unbounded domain. When we use a domain-type solver to handle the boundary value problems, we have to truncate the unbounded domain. We also need some manipulations on the truncated boundary such as PML (Turkel & Yefet, 1998) to let the numerical solution satisfy the radiation condition. In this paper, we use the FMBEM (Greengard & Rokhlin, 1987; Rokhlin, 1985), which can deal appropriately with wave problems in unbounded domain, to solve the forward and adjoint problems. In this section, we briefly present the formulation

of the FMBEM for the forward problem. The adjoint problem can be solved in the exact same manner.

The forward problem in Equations (11)–(13) can be reformulated with the following boundary integral equation:

$$
\begin{pmatrix} \gamma_x^* w_p^{\text{in}} \\ w^{\text{in}} \\ \alpha_1 q^{\text{in}} \end{pmatrix} = \begin{pmatrix} \frac{1}{2}\mathcal{I} + \gamma_x^* \mathcal{X} & -\gamma_x^* \mathcal{D}_1 & \frac{1}{\alpha_1}\gamma_x^* \mathcal{S}_1 \\ \mathcal{X} & -(\mathcal{D}_1 + \mathcal{D}_2) & \frac{1}{\alpha_1}\mathcal{S}_1 + \frac{1}{\alpha_2}\mathcal{S}_2 \\ \alpha_1 \mathcal{X}' & -(\alpha_1\mathcal{N}_1 + \alpha_2\mathcal{N}_2) & (\mathcal{D}_1^T + \mathcal{D}_2^T) \end{pmatrix} \begin{pmatrix} \gamma_x^* w_p \\ w \\ \alpha_1 q \end{pmatrix} , \quad (53)
$$

where q and q^{in} are the normal derivative of the total field w and the incident field w^{in}, respectively. Also, $\mathcal{S}_i$, $\mathcal{D}_i$, $\mathcal{D}_i^T$ and $\mathcal{N}_i$ for $i = 1, 2$ are the integral operators, respectively, defined as follows:

$$
(\mathcal{S}_i q)(x) = \int_\Gamma G_i(x - y) q(y) \mathrm{d}S(y), \tag{54}
$$

$$
(\mathcal{D}_i u)(x) = \int_\Gamma \frac{\partial G_i(x - y)}{\partial n(y)} u(y) \mathrm{d}S(y), \tag{55}
$$

$$
(\mathcal{D}_i^T q)(x) = \int_\Gamma \frac{\partial G_i(x - y)}{\partial n(x)} q(y) \mathrm{d}S(y), \tag{56}
$$

$$
(\mathcal{N}_i u)(x) = \int_\Gamma \frac{\partial^2 G_i(x - y)}{\partial n(x)\partial n(y)} u(y) \mathrm{d}S(y), \tag{57}
$$

In the TE problem, $\mathcal{X}, \mathcal{X}'$ and γ_x^* are, respectively, defined as follows:

$$
(\mathcal{X} u)(x) = - \int_{\Gamma_p} \frac{\partial G_1(x - y)}{\partial n(y)} u(y) \mathrm{d}S(y), \tag{58}
$$

$$
(\mathcal{X}' u)(x) = - \int_{\Gamma_p} \frac{\partial^2 G_1(x - y)}{\partial n(x)\partial n(y)} u(y) \mathrm{d}S(y), \tag{59}
$$

$$
\gamma_x^* = 1. \tag{60}
$$

In TM mode, $\mathcal{X}, \mathcal{X}'$ and γ_x^* are defined as follows:

$$
(\mathcal{X} q)(x) = \int_{\Gamma_p} G_1(x - y) q(y) \mathrm{d}S(y), \tag{61}
$$

$$
(\mathcal{X}' q)(x) = \int_{\Gamma_p} \frac{\partial G_1(x - y)}{\partial n(x)} q(y) \mathrm{d}S(y), \tag{62}
$$

$$
\gamma_x^* = \frac{\partial}{\partial n(x)}. \tag{63}
$$

In Equation (53), the operator $\gamma_x^* \mathcal{A}$ is defined as:

$$
(\gamma_x^* \mathcal{A} u)(x) = \gamma_x^* (\mathcal{A} u)(x), \tag{64}
$$

for an operator $\mathcal{A}$. Also, G_i is the fundamental solution of the Helmholtz equation defined as follows:

$$G_i(x - y) = \frac{i}{4} H_0^{(1)}(k_i |x - y|), \tag{65}$$

where $i = \sqrt{-1}$ and $H_n^{(1)}$ is the Hankel function of the first kind and nth order. The boundary integral Equation (53) is known as the PMCHWT formulation (Chew, 1995) which has the unique solution.

Krylov-based algebraic solvers require a (fast) evaluation technique of the integrals (54)–(57), (58), (59), (61) and (62) which is carried out by the fast multipole method (FMM) (Greengard & Rokhlin, 1987; Rokhlin, 1985) in this paper. The FMM is summarised in what follows. We are now interested in evaluating the following integral $\psi(x)$:

$$\psi(x) = \int_S G_i(x - y) q(y) dS(y), \tag{66}$$

where S is a subset of Γ which is far from the evaluation point x. We take a point X near x, and a point Y near y which satisfy the following relation:

$$|x - X + Y - y| < |X - Y|. \tag{67}$$

With these settings, the fundamental solution (65) can be expanded as follows:

$$G_i(x - y) = \frac{i}{4} \sum_{m=-\infty}^{\infty} \sum_{k=-\infty}^{\infty} (-1)^m O_{-k-m}(\overrightarrow{YX}) I_m(\overrightarrow{Yy}) I_k(\overrightarrow{Xx}), \tag{68}$$

where I_n and O_n are the entire solutions of Helmholtz' equation and radiating solutions of Helmholtz' equation which are singular at the origin, respectively. By substituting (68) into (66), we obtain the following local expansion of $\psi(x)$:

$$\psi(x) = \frac{i}{4} \sum_{k=-\infty}^{\infty} I_k(\overrightarrow{Xx}) L_{-k}(X), \tag{69}$$

where L_{-k} is the coefficient of the local expansion as follows:

$$L_{-k}(X) = \sum_{m=-\infty}^{\infty} O_{-k-m}(\overrightarrow{YX}) M_m(Y), \tag{70}$$

where M_m is the multipole moment as follows:

$$M_m(Y) = (-1)^m \int_S I_m(\overrightarrow{Yy}) q(y) dS(y). \tag{71}$$

Equation (70) is called the M2L formula. The FMM algorithm requires us to move the multipole moment and the coefficient of the local expansion, which is achieved by the following formulae:

$$M_\ell(Y') = \sum_{m=-\infty}^{\infty} I_{\ell-m}(\overrightarrow{YY'})M_m(Y), \tag{72}$$

$$L_\ell(X') = \sum_{m=-\infty}^{\infty} I_{\ell-m}(\overrightarrow{XX'})L_m(X). \tag{73}$$

Equations (72) and (73) are called M2M and L2L formula, respectively. All infinite sums in (70), (72) and (73) are appropriately truncated in numerical experiments according to the wave number (Ohnuki & Chew, 2003). In the implementation of the FMM, a hierarchical quad tree is utilised to let X, Y, x and y satisfy Equation (67).

We can now compute RHS of (53) for a given boundary data since evaluation of Equations (54)–(57), (58), (59), (61) and (62) can be done in a similar manner as the above procedure. Hence, we can now solve the algebraic equations obtained as discretised Equation (53) using an iterative solver. Once we obtain the solution (w and q) in (53), w and its derivative in the fixed design domain D which are required to evaluate the topological derivative, can be evaluated by the following representation:

$$w(x) = \delta_{i1}w^{\text{in}}(x) + (\mathcal{S}_i q)(x) - (\mathcal{D}_i u)(x) + (\mathcal{X}\gamma_x^* w_p)(x) \quad x \in \Omega_i, \tag{74}$$

$$\frac{\partial w(x)}{\partial x_j} = \delta_{i1}\frac{\partial w^{\text{in}}}{\partial x_j}(x) + \frac{\partial(\mathcal{S}_i q)}{\partial x_j}(x) - \frac{\partial(\mathcal{D}_i u)}{\partial x_j}(x) + \frac{\partial(\mathcal{X}\gamma_x^* w_p)}{\partial x_j}(x) \quad x \in \Omega_i, \tag{75}$$

which can also be evaluated with the FMM.

3. A level set-based topology optimisation

In this section, we present a topology optimisation method with the level set function and the topological derivative presented in the previous section.

3.1. Optimisation problem and associated level set method

Our objective is to find a shape and a topology of $\Omega_2 \subset D$ which minimise the multi-objective functional (24), where D is a bounded fixed design domain. To this end, we here utilise the level set-based topology optimisation (Sethian & Wiegmann, 2000). The level set method can be classified into two types, one of which utilises the shape derivative (Allaire, Jouve, & Toader, 2004; Sethian & Wiegmann, 2000; Wang et al., 2003) while the other utilises the topological derivative (Amstutz & Andrä, 2006; Burger, Hackl, & Ring, 2004; He, Kao, & Osher, 2007; Yamada et al., 2010). In this paper, we adopt the latter type of optimisation since it can naturally deal with topological changes. We specifically

use the one proposed by Yamada et al. (2010), which employs the reaction-diffusion equation to evolve the level set function. The level set function, denoted as $\phi(x)$, is defined as follows:

$$\begin{cases} 0 < \phi(x,t) \le 1 & \forall x \in \Omega_1(t), \\ 0 = \phi(x,t) & \forall x \in \Gamma(t), \\ -1 \le \phi(x,t) < 0 & \forall x \in \Omega_2(t), \end{cases} \tag{76}$$

where t is a fictitious time which corresponds to an optimisation step. With the help of the level set function (76), our optimisation problem is defined as 'Find an optimal distribution of ϕ which minimises $\mathcal{J}$ in Equation (24) subject to both TE and TM problems'. Since the optimisation problem is difficult to solve directly, we explore the optimum distribution of ϕ from an initial guess ϕ_0 by the following time evolution equation:

$$\frac{\partial \phi(x,t)}{\partial t} = \text{sgn}(\phi(x,t))C\mathcal{T}(x,t) + \tau \ell^2 \Delta \phi(x,t) \quad x \in D, \ t \in \mathbb{R}^+, \tag{77}$$

$$\phi(x,0) = \phi_0(x) \quad x \in D, \tag{78}$$

where $C > 0$ is a constant, ℓ is a characteristic length of D and $\tau > 0$ is a regularisation parameter. The first term of RHS of the evolution Equation (77) works to decrease the objective functional (49). When the topological derivative at $x \in \Omega$ is negative, it is favourable to put a scatterer at x. This can be achieved by decreasing ϕ in the case that x is located in Ω_1, and by increasing ϕ in the case that x is located in Ω_2. The second term of RHS of Equation (77) is a regularisation term, which prohibits a sharp spatial change of the level set function. When ϕ is concave up in the neighbourhood of x, $\phi(x)$ is increased. We also introduce a boundary condition on ∂D for ϕ to limit Ω_2 inside D as follows:

$$\phi(x,t) = d \quad x \in \partial D, \tag{79}$$

where d is a positive constant. Note that the initial-boundary value problem for the evolution of the level set function (77), (78) and (79) can appropriately be solved by a domain-type solver such as the FEM since the problem is defined on the bounded domain D and D is irrelevant to the fictitious time t. Solving the evolution Equation (77) by the BEM is possible but not efficient since Equation (77) involves the source term (the first term in RHS). In this case, a domain mesh is required even when the BEM used. Hence, in the present study, the FEM is employed to solve the evolution equation.

3.2. Meshing procedure

In order to run the FMBEM for the calculation of the topological derivative $\mathcal{T}$ in Equation (77), it is required to generate boundary element mesh corresponding to the distribution of the level set function. In this subsection, the meshing procedure is presented.
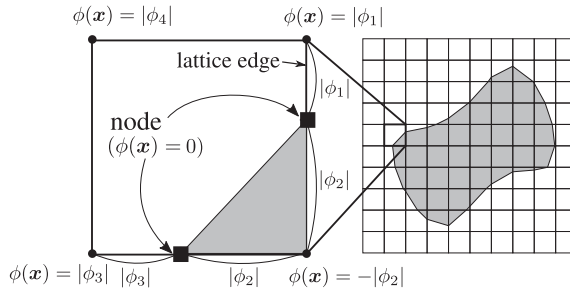
Figure 2. Generation of the boundary mesh.
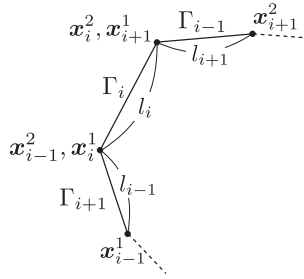
Figure 3. Definition of symbols related to boundary elements.

The value of the level set function is stored on a grid point of lattice expanding the design domain D. We explore a set of nodes X^{node} of boundary elements defined as $X^{\text{node}} = \{x|\phi(x) = 0$ and x is on a lattice edge$\}$ by linearly interpolating the value of the level set function ϕ on the lattice edge (Figure 2). By connecting the nodes $x \in X^{\text{node}}$, we have n boundary elements denoted as Γ_i $(i = 1, \ldots, n)$. With this construction, the minimum value of the length of the boundary elements are not necessarily bounded from below, which may give an ill-conditioned coefficient matrix. In order to avoid this situation, we improve the boundary mesh by the following strategy. Let us denote the length of Γ_i as l_i, and nodes of Γ_i as x_i^1 and x_i^2 for $i = 1, \ldots, n$ as in Figure 3. Using the Ferguson curve, the interval between x_i^1 and x_i^2 are interpolated as follows:

$$x(u) = (2u^3 - 3u^2 + 1)x_i^1 + (-2u^3 + 3u^2)x_i^2 + (u^3 - 2u^2 + u)t_i^1 + (u^3 - u^2)t_i^2, \tag{80}$$

where $u \in [0, 1]$ is a local coordinate and t_i^1 and t_i^2 are tangent vectors at x_i^1 and x_i^2, respectively. t_i^1 and t_i^2 are evaluated as follows:

$$t_i^1 = \frac{l_i(x_{i-1}^2 - x_{i-1}^1)}{l_{i-1}}, \tag{81}$$

$$t_i^2 = \frac{l_i(x_{i+1}^2 - x_{i+1}^1)}{l_{i+1}}. \tag{82}$$

We improve the boundary mesh using the Ferguson curve. First, we search boundary elements Γ_i whose length l_i is less than a preset value l_s. When l_i satisfies the condition, we eliminate Γ_i by merging x_i^1 and x_i^2 to $x(0.5)$ (Figure 4 left). We henceforth denote the length of the shortest edge after applying this process to all of the boundary elements as l_{min}. Second, we divide each boundary element into c parts by putting new nodes at $u = 1/c, \ldots, (c-1)/c$ on the Ferguson curve (80). c is a constant defined as follows:

$$c = \left[\frac{c_{div} l_i}{l_{min}} \right] \quad (i = 1, \ldots, n), \tag{83}$$

where c_{div} is a constant with which fineness of the mesh is defined and $[x]$ represents the largest integer which is smaller than x. For instance, in the case of $c = 2$, the point $x(0.5)$ is added as a new node (Figure 4 right). By following this procedure, the length of each boundary element will be about the same degree of l_{min}/c_{div}.

3.3. Algorithm

Combining all techniques presented above, the algorithm of the proposed topology optimisation is summarised as follows:

(1) The fixed design domain D is divided into finite elements.
(2) An initial distribution of the level set function ϕ_0 is given on nodes of the finite elements.
(3) Boundary elements are generated from the distribution of ϕ by the procedure presented in Section 3.2.
(4) The forward boundary value problem in Equations (11)–(15) is solved by the FMBEM presented in Section 2.3.
(5) The objective functional is evaluated by the FMBEM. When the objective function converges, stop.
(6) The adjoint boundary value problem in Equations (39)–(43) is solved by the FMBEM presented in Section 2.3.
(7) Topological derivative in Equation (48) is evaluated on the nodes of the finite elements.
(8) Distribution of the level set function ϕ is obtained as the solution of the boundary value problem in Equations (77), (78) and (79) by the FEM. Go to 3.

4. Numerical experiments

In this section, we present some numerical examples to show the validity and the efficiency of the proposed method. We first state common issues for all examples:

- The boundary integral Equation (53) is discretised with the constant element.
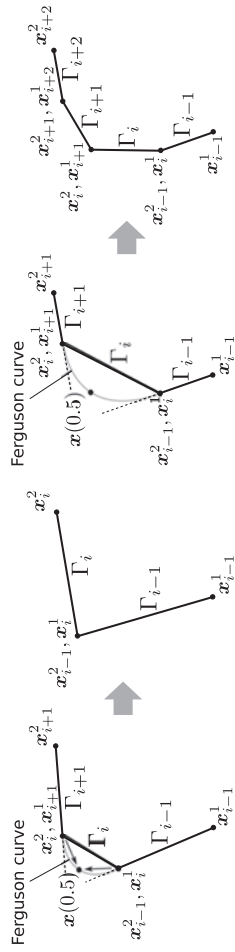
Figure 4. (Left:) Elimination of a short boundary element, (right:) Division of a boundary element in the case that $c = 2$.
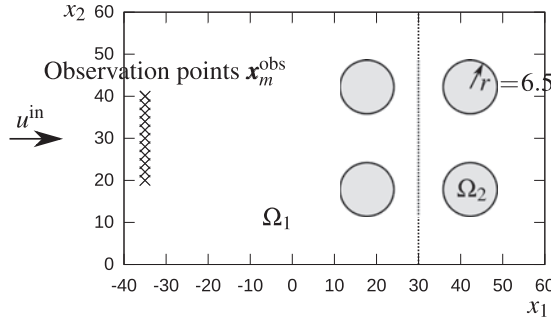
Figure 5. Settings for the verification of the topological derivatives (50) and (52).

- To solve algebraic equations involved in the BEM, we used GMRES whose tolerance is set to be 10^{-10}.
- Rectangular isoparametric finite elements are used to solve the evolution Equation (77). The number of the finite elements is approx. 10,000.

4.1. Verification of the topological derivative

We first check the validity of the topological derivative (48) of the composite objective functional (24). In this example, we consider the settings in Figure 5, i.e. four dielectric materials Ω_2 of $\varepsilon_2 = 3$ are set in the host dielectric material with $\varepsilon_1 = 1$, the incident wave is set as the plane wave with frequency $\omega = 0.5$ propagating in x_1 direction. The objective functionals are defined as the sum of the intensity of electric (J_m) and magnetic (J_e) fields on observation points $x_m^{obs} = \{x | x_1 = -35, x_2 = 20 + 2m\}$ ($m = 1, \ldots, 10$) as:

$$J_e = \frac{1}{2} \sum_{m=1}^{10} |u(x_m^{obs})|^2, \tag{84}$$

$$J_m = \frac{1}{2} \sum_{m=1}^{10} |v(x_m^{obs})|^2. \tag{85}$$

With these settings, we have computed the topological derivatives of the weighted sum (49) and the KS function (51) of J_e and J_m with $c_e = c_m = 1$. As a reference solution, we calculated the 'topological difference $\mathcal{D}$', which is calculated in the following procedure:

(1) The objective function is calculated for the initial configuration of $\Omega_1 \cup \Omega_2$. The calculated objective function is denoted as J_{before}.
(2) A small spherical scatterer Ω_r of radius $r = 0.05$ is introduced in $\Omega_1 \cup \Omega_2$. The objective function is calculated for $(\Omega_1 \cup \Omega_2) \setminus \overline{\Omega}_r$. The calculated objective function is denoted as J_{after}.
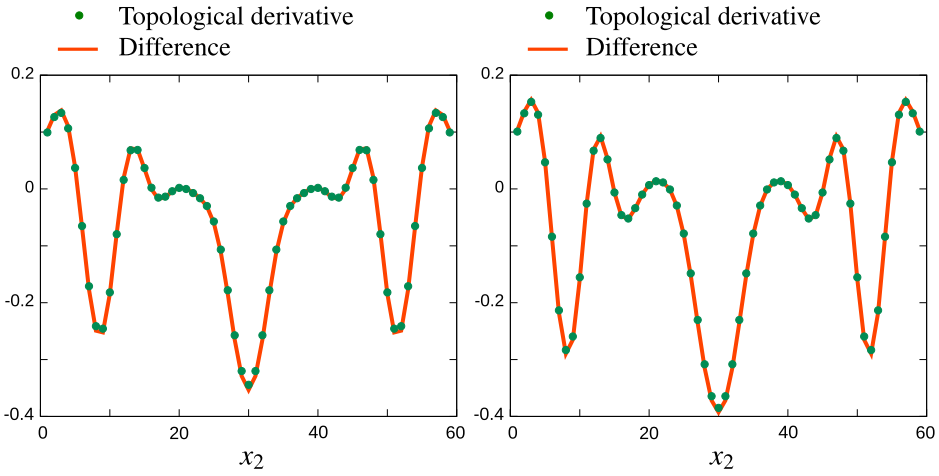
Figure 6. Topological derivatives of (left:) the weighted sum (right:) the KS function.

(3) The topological difference $\mathcal{D}$ is calculated as follows:

$$\mathcal{D} = \frac{J_{\text{after}} - J_{\text{before}}}{\pi r^2}. \qquad (86)$$

For this experiment, we used the conventional BEM without FMM because the difference between J_{before} and J_{after} is tiny. To keep significant digits of the difference $J_{\text{after}} - J_{\text{before}}$, it is crucially important to calculate J_{before} and J_{after} in a considerably accurate manner. We typically need to calculate J_{before} and J_{after} in 10-digits accuracy or more. On the other hand, the accuracy for the FMM is controled by the truncation number for the infinite sums involved in the formulations for the FMM (Equations (69), (70), (72) and (73)). When we try to guarantee the 10-digits accuracy for the FMM, the computational efficiency of the FMM is less than that of the conventional BEM due to the huge truncation number for the infinite sums. Hence, we have chosen to use the conventional BEM to validate the topological derivative with the topological difference.

In Figure 6, we have plotted the topological derivatives $\mathcal{T}_{\text{sum}}$ and $\mathcal{T}_{\text{KS}}$ on $x_1 = 30$ along with the topological difference $\mathcal{D}$. We observe that the topological derivatives agree well with the references, from which we confirm the validity of the topological derivative of the composite function calculated by the chain rule in Equation (48).

4.2. Optimisation of dielectric materials with perturbed permittivity

In this section, we consider a topology optimisation problem in Figure 7 to find $\Omega_2 \subset D = [0, 90] \otimes [0, 90]$ which minimises the following 10 objective functions simultaneously:
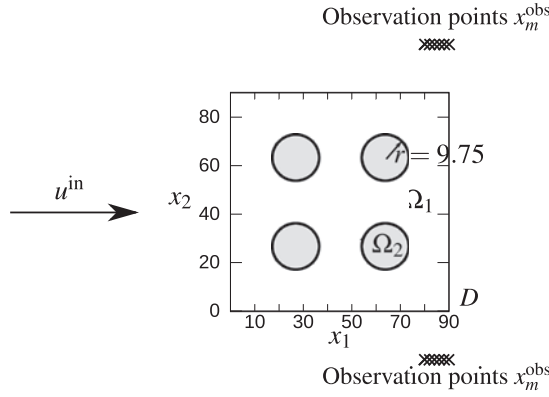
Figure 7. Settings for the perturbed permittivity problem.

$$J_{\mathrm{e}}^{(i)} = \frac{1}{2} \sum_{m=1}^{M} |u^{(i)}(x_m^{\mathrm{obs}})|^2 \quad (i = 1, \ldots, 5), \tag{87}$$

$$J_{\mathrm{m}}^{(i)} = \frac{1}{2} \sum_{m=1}^{M} |v^{(i)}(x_m^{\mathrm{obs}})|^2 \quad (i = 1, \ldots, 5), \tag{88}$$

where $u^{(i)}$ for $i = 1, 2, 3, 4$ and 5 are the solutions of the TE problem in Equations (1)–(5) with $\varepsilon_1 = 1.0$ and $\varepsilon_2 = 2.0, 2.5, 3.0, 3.5$ and 4.0, respectively. Also, $v^{(i)}$ is the TM counterpart of $u^{(i)}$. x_m^{obs} are 12 observation points set as $x_m^{\mathrm{obs}} = \{x_m^{\mathrm{obs}}|x_1 = 80 + 2n \text{ for } n = 0, \ldots, 6, \ x_2 = -20 \text{ and } 110\}$. As the incident wave, plane wave with frequency $\omega = 0.333$ propagating in x_1 direction is used. This model is regarded as a problem to find an allocation of dielectric material(s) which minimises the intensity of both electric and magnetic fields regardless of the permittivity of the dielectric material(s) to be used. To deal with the multiple objective functions (87) and (88), we consider the weighted sum and the KS function of $J_{\mathrm{e}}^{(i)}$ and $J_{\mathrm{m}}^{(i)}$. An optimal distribution of Ω_2 is explored from the initial guess indicated in Figure 7, i.e. four dielectric materials of radius $r = 9.75$. Although we have used non-dimensional variables, one can appropriately convert the variables to ones with units. For example, when the radius of the initial dielectric rod $r = 9.75$ is assumed to be $r = 487.5\,\mathrm{mm}$, the frequency of the incident wave corresponds to 0.5 GHz (microwave).

Figure 8 shows the obtained configurations in the case of the weighted sum and the KS function. In both cases, the topology of the dielectric materials has changed from that of the initial guess (Figure 7). As a reference, we have solved single-objective optimisation problems, i.e. an allocation of dielectric material(s) Ω_2 which minimises either $J_{\mathrm{e}}^{(3)}$ or $J_{\mathrm{m}}^{(3)}$ (Figure 9). One observes that the obtained configurations for the single-objective optimisation problems are considerably different from ones for the multi-objective optimisation problems (Figure 8). In what follows, we examine the performance of each configuration.
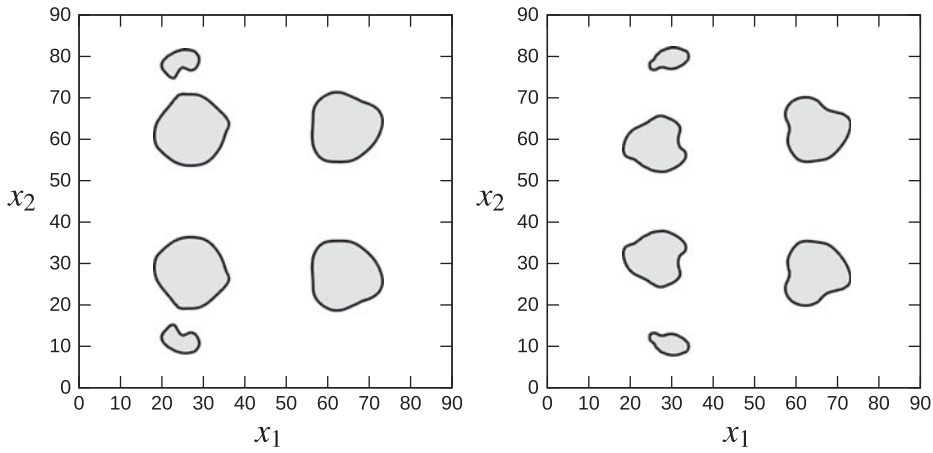
Figure 8. Obtained optimal configurations for (left:) the weighted sum (right:) the KS function.
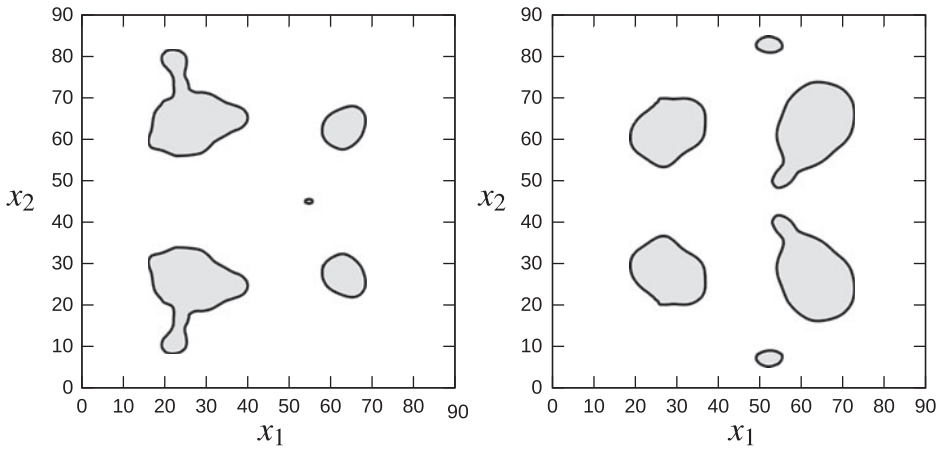
Figure 9. Optimal configurations to minimise (left:) $J_m^{(3)}$ (right:) $J_m^{(3)}$.

Figure 10 shows the sum of the intensity of electric and magnetic fields on the observation points against ε_2. While the single-objective optimisation can effectively decrease the intensity by the specific dielectric material of $\varepsilon_2 = 3.0$, the performance for other materials of different permittivity is not sufficient. For materials with larger permittivity, the intensity is even increased compared with the initial value in the case of the single-objective problem. For the case that the multi-objective optimisations are used, although the intensity with $\varepsilon_2 = 3.0$ is slightly larger than the single-objective one, the intensity is decreased for wide range of ε_2. Especially, when the KS function is employed, the obtained curves are almost flat, from which it is concluded that the KS function is effective when the multiple objective functions are concerned.
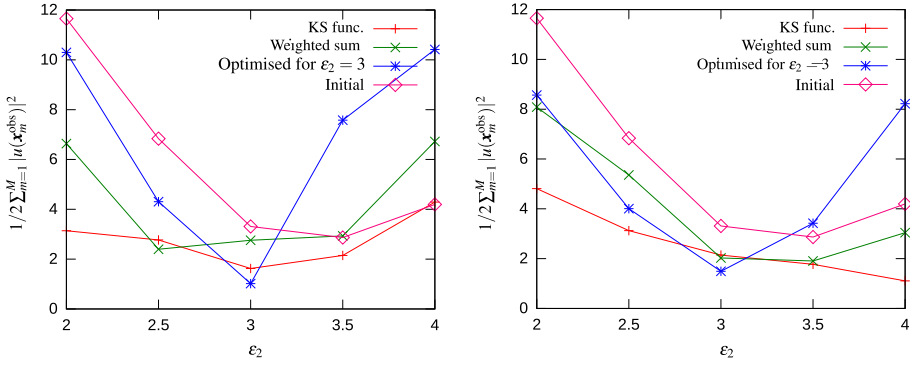
Figure 10. Objective functional values vs ε_2 for the case of (left:) TM mode (right:) TE mode.
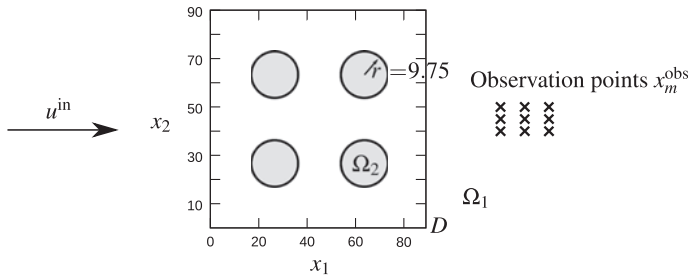
4.3. Wideband optimisation

We next consider another multi-objective topology optimisation problem in Figure 11 to find $\Omega_2 \subset D = [0, 90] \otimes [0, 90]$ which minimises the following 6 objective functionals simultaneously:

$$J_e^{(i)} = \frac{1}{2} \sum_{m=1}^{M} |u^{(i)}(x_m^{\mathrm{obs}})|^2 \quad (i = 1, \ldots, 3), \tag{89}$$

$$J_m^{(i)} = \frac{1}{2} \sum_{m=1}^{M} |v^{(i)}(x_m^{\mathrm{obs}})|^2 \quad (i = 1, \ldots, 3), \tag{90}$$

where $u^{(i)}$ for $i = 1, 2$ and 3 are the solutions of TE problem in Equations (1)–(5) with $\omega = 3.0, 4.0$ and 5.0, respectively. Also $v^{(i)}$ is the TM counterpart of $u^{(i)}$. x_m^{obs} are 12 observation points set as $x_m^{\mathrm{obs}} = \{x_m^{\mathrm{obs}} | x_1 = 120 + 10j$ for $j = 0, 1, 2, x_2 = 40 + 5k$ for $k = 0, 1, 2\}$. As the incident wave, plane wave with frequency ω propagating in x_1 direction is used. The initial guess of the allocation of dielectric materials are the same with the ones in the previous subsection. For this example, only the KS function of the objective functions (89) and (90), with $c_e = c_m = 1$, is concerned since the effectiveness of the KS function is already confirmed in the previous subsection. Figure 12 shows the obtained configuration which minimises the KS function of (89) and (90). The topology of the obtained configuration is different from the initial guess (Figure 11). Table 1 shows the objective functions, and Figures 13 and 14 show the electric intensity of TM mode and the magnetic intensity of TE mode around the design domain D, respectively. One observes that the obtained configuration of the dielectric materials (Figure 12) can decrease the intensity of the fields on the observation points for all frequencies concerned. With these observations, we conclude that the proposed methodology can appropriately deal with wideband optimisation problems.

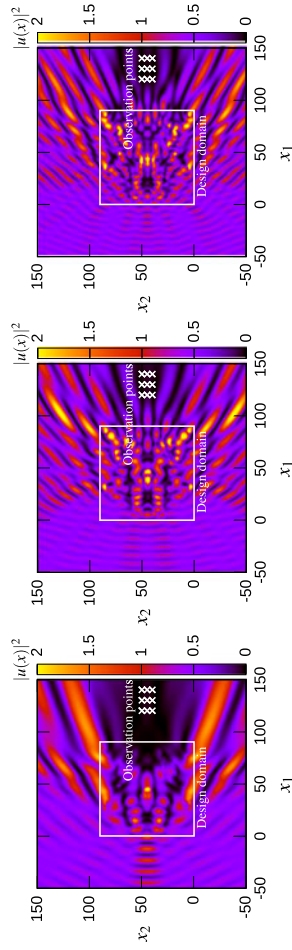**Figure 11.** Settings for the wideband optimisation problem.
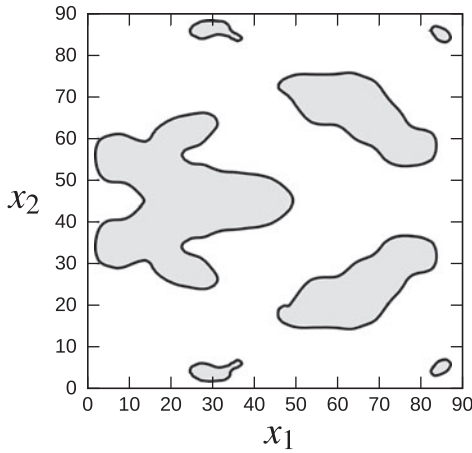
Figure 12. Optimal configuration for the wideband optimisation problem.

Table 1. Objective functions for the initial and optimised configurations in the case of the wideband optimisation.

	Initial			Optimised		
	$\omega = 0.3$	$\omega = 0.4$	$\omega = 0.5$	$\omega = 0.3$	$\omega = 0.4$	$\omega = 0.5$
TE	6.361	6.856	2.302	0.2067	0.2692	0.1508
TM	7.673	7.299	3.077	0.7555	0.2694	0.1948

4.4. Optimal design of a cloaking device for both TE and TM modes

To show that the proposed method can also effectively solve a relatively complicated problem, we consider an optimal design of a cloaking material. We here define the optimisation for the cloaking design as to find an optimal configuration of the dielectric material which minimises the KS function (51) of the following

Figure 13. Intensity of the electric fields (TM mode) with the optimised configuration for the wideband optimisation problem. For the case that the plane wave with (left:) $\omega = 3.0$, (centre:) $\omega = 4.0$, (right:) $\omega = 5.0$ impinges on the optimised shaped dielectric materials.
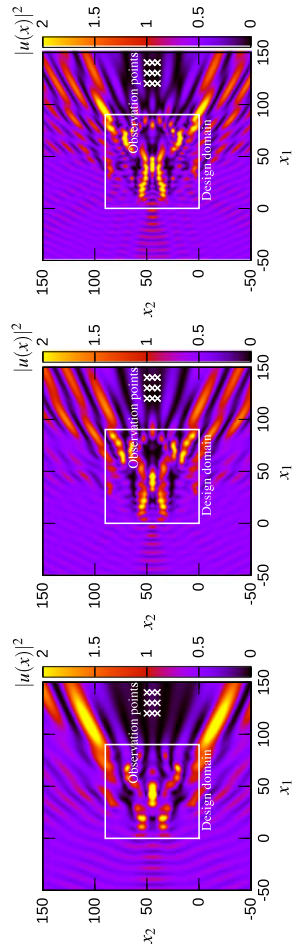
Figure 14. Intensity of the magnetic fields (TE mode) with the optimised configuration for the wideband optimisation problem. For the case that the plane wave with (left:) $\omega = 3.0$, (centre:) $\omega = 4.0$, (right:) $\omega = 5.0$ impinges on the optimised shaped dielectric materials.
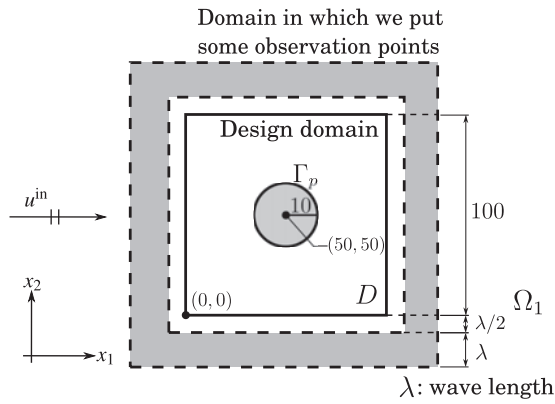
Domain in which we put
some observation points

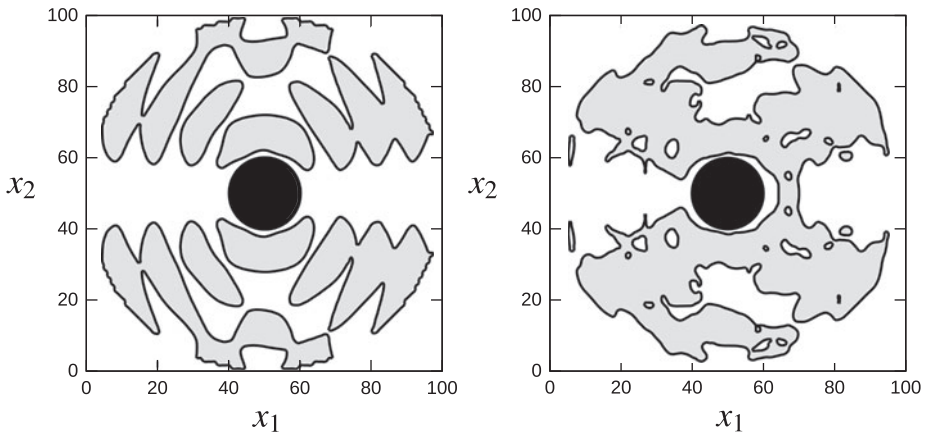**Figure 15.** Settings for the cloaking problem.

Figure 16. (Left:) Initial (right:) optimal configuration. The black circle represents the PEC to be cloaked. Grey coloured domains represent dielectric materials.
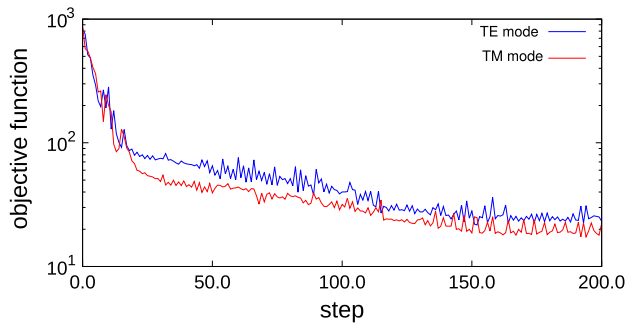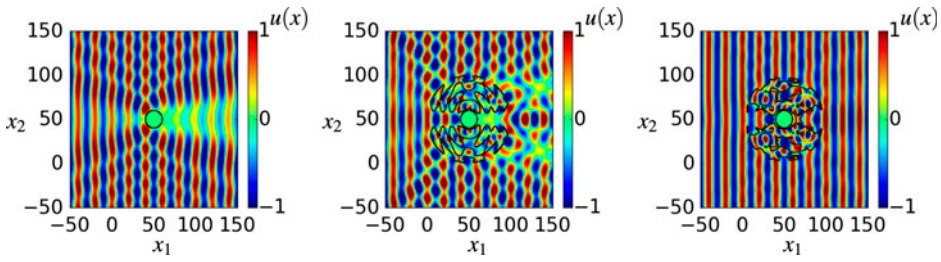

Figure 17. History of the objective functional for the cloaking problem.

Figure 18. Electric fields (TM mode) for (left:) bare PEC, (right:) initial configuration, (left:) optimal configuration.

functionals J_e and J_m:

$$J_e = \sum_{m=1}^{M} |u(x_m^{obs}) - u^{in}(x_m^{obs}))|^2, \tag{91}$$

$$J_m = \sum_{m=1}^{M} |v(x_m^{obs}) - v^{in}(x_m^{obs}))|^2, \tag{92}$$

where u and v are, respectively, the solution of the TE in Equations (1)–(5) and TM in Equations (6)–(10) problem with a circular PEC Ω_p of radius $r = 10$ located at $(50, 50)$ and dielectric materials of $(\varepsilon_1, \varepsilon_2) = (1.0, 3.0)$. The incident wave is defined as a plane wave with frequency $\omega = 0.314$ propagating in x_1 direction. Also, the observation points are collocated in equal interval $\lambda/10$ in a grey area in Figure 15, where $\lambda = 20$ is the wave length of the incident wave. These settings are considered as design of cloaking for visible light. Indeed, for example, when the radius of the PEC $r = 10$ is assumed to be $r = 283.5$ nm, the frequency of the incident wave corresponds to 628.5 THz. Total number of the observation points ends up with $M = 2290$ with this setting. The objective functionals (91) and (92) indicate that the intensity of scattering fields by the PEC Ω_p is minimised in this optimisation problem.

Since, for this problem, the shape of the PEC Ω_p does not change in the optimisation process, the design domain D is defined as $D = ([0, 100] \otimes [0, 100]) \setminus \overline{\Omega_p}$. An optimal configuration of $\Omega_2 \subset D$ is explored from the initial configuration in the left figure of Figure 16. The initial configuration of dielectric materials is set by putting dielectric materials where the topological derivative (52) for the case of $\Omega_2 = \emptyset$ is negative. After 200 steps of the optimisation process, an optimal configuration in the right figure of Figure 16 is obtained.

Figure 17 shows the convergence history of each objective functional. Both objective functionals are decreased to comparable level. Figures 18 and 19, respectively, show electric and magnetic fields around the design domain for the case without cloaking, for initial configuration and for the obtained cloak.
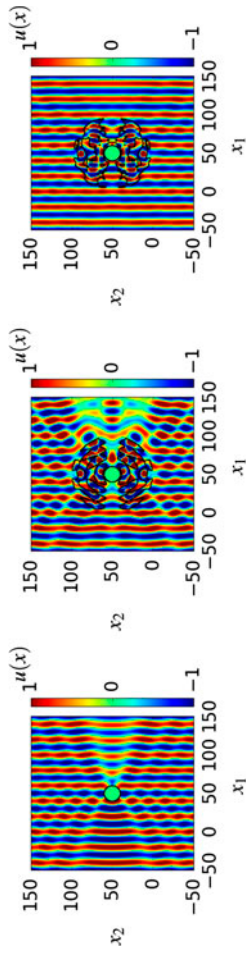
Figure 19. Magnetic fields (TE mode) for (left:) bare PEC, (right:) initial configuration, (left:) optimal configuration.

One observes that the scattering from the PEC is reduced by the obtained cloak, and plane incident wave is reconstructed by the cloak in the right figures.

5. Conclusions

We have presented a topology optimisation method to find an optimal configuration of dielectric material(s) which minimises some objective functionals simultaneously. We have shown that the composite functional of objective functions can appropriately evaluated with the chain rule. After the topological derivative is validated with a numerical experiment with the FMBEM, we have shown some numerical examples with the level set method in which some objective functions are minimised simultaneously. We have shown that the proposed methodology can be used to solve wideband optimisation problem, optimal design problem of cloaking, etc. Although we have restricted ourselves to two-dimensional electromagnetic wave problems, the proposed methodology can straightforwardly be used in other fields of engineering, including acoustics, elasticity and thermal problems in two- or three-dimensions.

Disclosure statement

No potential conflict of interest was reported by the authors.

Funding

ORCID

Hiroshi Isakari http://orcid.org/0000-0002-7906-5477
Kenta Nakamoto http://orcid.org/0000-0003-0954-7320
Tatsuya Kitabayashi http://orcid.org/0000-0002-7985-1435

References

Abe, F., Isakari, H., Takahashi, T., & Matsumoto, T. (2013). A topology optimisation in two-dimensional electromagnetics with the level set method and the boundary element method (in Japanese). *Transactions of JASCOME, 13*, 37–42.

Allaire, G., Jouve, F., & Toader, A. M. (2004). Structural optimization using sensitivity analysis and a level-set method. *Journal of Computational Physics, 194*, 363–393.

Amstutz, S., & Andrä, H. (2006). A new algorithm for topology optimization using a level-set method. *Journal of Computational Physics, 216*, 573–588.

Bendsøe, M. P., & Kikuchi, N. (1988). Generating optimal topologies in structural design using a homogenization method. *Computer Methods in Applied Mechanics and Engineering, 71*, 197–224.

Bonnet, M., & Nemitz, N. (2007). FM-BEM and topological derivative applied to acoustic inverse scattering. In M. Schanz, & O. Steinbach (Eds.), *Boundary element analysis* (pp. 187–212). Berlin, Heidelberg: Springer.

Burger, M., Hackl, B., & Ring, W. (2004). Incorporating topological derivatives into level set methods. *Journal of Computational Physics, 194*, 344–362.

Byun, J. K., & Park, I. H. (2007). Design of dielectric waveguide filters using topology optimization technique. *IEEE Transactions on Magnetics, 43*, 1573–1576.

Carpio, A., & Rapún, M. L. (2008). Solving inhomogeneous inverse problems by topological derivative methods. *Inverse Problems, 24*, 045014.

Chew, W. C. (1995). *Waves and fields in inhomogeneous media* (Vol. 522). New York, NY: IEEE Press.

Greengard, L., & Rokhlin, V. (1987). A fast algorithm for particle simulations. *Journal of Computational Physics, 73*, 325–348.

He, L., Kao, C. Y., & Osher, S. (2007). Incorporating topological derivatives into shape derivatives based level set methods. *Journal of Computational Physics, 225*, 891–909.

Isakari, H., Kuriyama, K., Harada, S., Yamada, T., Takahashi, T., & Matsumoto, T. (2014). A topology optimisation for three-dimensional acoustics with the level set method and the fast multipole boundary element method. *Mechanical Engineering Journal, 1*, CM0039. https://www.jstage.jst.go.jp/article/mej/1/4/1_2014cm0039/_article

Jensen, J. S. (2007). Topology optimization problems for reflection and dissipation of elastic waves. *Journal of Sound and Vibration, 301*, 319–340.

Jing, G., Isakari, H., Matsumoto, T., Yamada, T., & Takahashi, T. (2015). Level set-based topology optimization for 2d heat conduction problems using bem with objective function defined on design-dependent boundary with heat transfer boundary condition. *Engineering Analysis with Boundary Elements, 61*, 61–70.

Kondo, T., Isakari, H., Takahashi, T., & Matsumoto, T. (2014). A topology optimisation in 3d-acoustics for scatterers with impedance boundaries with the level set method and the fast multipole boundary element method (in Japanese). *Transactions of JASCOME, 14*, 29–24.

Kourogi, Y., Isakari, H., Takahashi, T., Yamada, T., & Matsumoto, T. (2013). On a topological sensitivity analysis of three-dimensional electromagnetic wave problems with the boundary element method and its application to a level set based structural optimization (in Japanese). *Transactions of JASCOME, 13*, 55–60.

Novotny, A. A., Feijóo, R. A., Taroco, E., & Padra, C. (2003). Topological sensitivity analysis. *Computer Methods in Applied Mechanics and Engineering, 192*, 803–829.

Novotny, A. A., Feijóo, R. A., Taroco, E., & Padra, C. (2007). Topological sensitivity analysis for three-dimensional linear elasticity problem. *Computer Methods in Applied Mechanics and Engineering, 196*, 4354–4364.

Ohnuki, S., & Chew, W. C. (2003). Numerical accuracy of multipole expansion for 2d mlfma. *IEEE Transactions on Antennas and Propagation, 51*, 1883–1890.

Otomori, M., Yamada, T., Andkjaer, J., Izui, K., Nishiwaki, S., & Kogiso, N. (2013). Level set-based topology optimization for the design of an electromagnetic cloak with ferrite material. *IEEE Transactions on Magnetics, 49*, 2081–2084.

Papoutsis-Kiachagias, E. M., & Giannakoglou, K. C. (2015). Continuous adjoint methods for turbulent flows, applied to shape and topology optimization: Industrial applications. *Archives of Computational Methods in Engineering, 23*, 255–299.

Rokhlin, V. (1985). Rapid solution of intergral equations of classical potential theory. *Journal of Computational Physics, 60*, 187–207.

Sethian, J. A., & Wiegmann, A. (2000). Structural boundary design via level set and immersed interface methods. *Journal of Computational Physics, 163*, 489–528.

Turkel, E., & Yefet, A. (1998). Absorbing PML boundary layers for wave-like equations. *Applied Numerical Mathematics, 27*, 533–557.

Wang, M. Y., Wang, X., & Guo, D. (2003). A level set method for structural topology optimization. *Computer Methods in Applied Mechanics and Engineering, 192*, 227–246.

Yaji, K., Yamada, T., Yoshino, M., Matsumoto, T., Izui, K., & Nishiwaki, S. (2014). Topology optimization using the lattice boltzmann method incorporating level set boundary expressions. *Journal of Computational Physics, 274*, 158–181.

Yamada, T., Izui, K., & Nishiwaki, S. (2011). A level set-based topology optimization method for maximizing thermal diffusivity in problems including design-dependent effects. *Journal of Mechanical Design, 133*, 031011.

Yamada, T., Izui, K., Nishiwaki, S., & Takezawa, A. (2010). A topology optimization method based on the level set method incorporating a fictitious interface energy. *Computer Methods in Applied Mechanics and Engineering, 199*, 2876–2891.